Journal of Nanostructure in Chemistry (2018) 8:189–196
https://doi.org/10.1007/s40097-018-0266-5

ORIGINAL RESEARCH

Preparation of inorganic–organic nanohybrid compound based on Ni^{II}, MoO_3 and *p*-phenylenediamine by hydrothermal method and its photoluminescence property

R. Ranjineh Khojasteh[1] · **S. Ghelenji**[1]

Received: 13 February 2018 / Accepted: 30 May 2018 / Published online: 8 June 2018
© The Author(s) 2018

Abstract
The new nanocrystalline composition was synthesized using $NiSO_4$ and MoO_3 and PPDA (*p*-phenylenediamine) via the hydrothermal method. The structure, morphology and photoluminescence property of nanocrystal were studied using X-ray diffraction (XRD), Fourier transform infra red (FT-IR) spectroscopy, scanning electron microscopy (SEM), photoluminescence (PL) spectra, thermogravimetric analysis (TGA–DTA) and energy-dispersive X-ray spectroscopy (EDX). The effect of factors such as type and concentration of initial materials, pH values, temperature and reaction duration on the structure and morphology of nanocrystals was investigated in the preparation of composition. The results show that the pH of the initial solution affects the size of the prepared nanocrystals; the size of the crystals is increased and the morphology of the nanostructures is changed with the increment in pH value. According to the obtained results, neutral or low alkaline conditions of pH are more favorable for the formation of the nanocrystals. The obtained nanocrystal shows an intense PL emission at room temperature with a maximum peak at 461 nm and excitation at the wavelength of 300 nm. TGA and DTA analysis display a total weight loss of 13.42%.

Keywords Hydrothermal · Nanocrystal · Ni · Mo · *p*-Phenylenediamine · Nanohybrid materials

Introduction

Due to the unique properties and characteristics of inorganic–organic nanohybrid materials in various industries, there is a great desire to prepare and study their applications. Surface and volumetric properties of inorganic–organic nanohybrids and the surface-to-volume ratio of these materials in the scale of nanometers have produced significant changes in them [1–5].

The engineering of nanocrystals of inorganic–organic hybrid materials is focused on the two aspects in terms of their structural flexibility [6] and, secondly, their application as a catalyst, as gas storage, as ion sieve, in photochemistry and in electromagnetism [7–14]. Hydrothermal crystallization in the presence of multifunctional organic amines is one of the methods widely used for the synthesis of these materials. Multifunctional organic nitrogen-containing ligands such as bipyridine (4,4′-byp) [15–17], ethylenediamine (en) [18, 19] and 1, 10-phenanthroline (phen) [20, 21] have large possibilities for the formation of 3D frameworks containing metal atoms. On the other hand, these frameworks can be coupled with oxomolybdates and can form semiconductor nanostructures [22] with novel applications in photoluminescence [23, 24], light harvesting [25, 26] and so on. PPDA as multifunctional organic ligand can be placed between structural blocks of oxomolybdates which are widely used in the structure of inorganic–organic nanohybrids as agents for structural directing to facilitate the formation of different networks [27]. These ligands can not only be used as coordination factors to transition metals, but also cause the formation of one-dimensional or multi-dimensional networks by forming intermolecular interactions, such as hydrogen bonding [28–31]. These compounds are commonly synthesized by the hydrothermal method in solid state at temperatures above 150 °C. The advantage of this method is that chemical homogeneity, morphology purity, shape and composition phase are controlled under moderate conditions and thus a

✉ R. Ranjineh Khojasteh
r_ranjinehkhojasteh@iau-tnb.ac.ir

[1] Department of Inorganic Chemistry, Faculty of Chemistry, Tehran North Branch, Islamic Azad University, Tehran 1651153311, Iran

nanocrystalline structure with different capabilities such as electrical properties is obtained.

Inorganic–organic hybrid materials composed of Mo and PPDA have been studied mostly in terms of crystal structure [32–34], but preparation of their nanoparticles has not been reported. Therefore, we were interested in synthesizing these nanoparticles and studying their structure and properties. In this article, the hydrothermal method has been used for the synthesis of $NiSO_4$ and MoO_3 nanostructure crystals using PPDA spacers. Herein, PPDA is chosen as the spacer group because it can be easily polymerized under neutral conditions, and the NH_2 donor sites within PPDA makes it suitable for the construction of an inorganic–organic nanohybrid. The effect of factors influencing the hydrothermal process and pH values on the morphology of nanocrystals as well as their luminescence properties has also been discussed.

Materials and methods

Materials and spectral measurements

All initial materials were purchased from Aldrich and Merck and used without further purification. Powder X-ray diffraction (PXRD) spectra were measured on a STOE-STADIP. Fourier transform infrared (FT-IR) was recorded in KBr discs on a Perkin-Elmer 78 spectrophotometer. Scanning electron microscopy (SEM) and energy-dispersive X-ray spectroscopy (EDX) were observed with EM 3200-KYKY. Photoluminescence (PL) spectra were obtained with a Perkin Elmer LS55 spectrometer using a 150 W xenon lamp as the excitation source. Thermogravimetric analysis (TGA–DTA) was performed on a BAHR STA 503 Thermal analyzer in air with a heating rate of 5 °C/min.

General method to prepare nanocrystals

A mixture of $NiSO_4.6H_2O$ (0.05 g, 0.190 mmol), MoO_3 (0.015 g, 0.104 mmol), PPDA (*p*-phenylenediamine) (0.011 g, 0.102 mmol) and distilled water (10 g, 555.5 mmol) with molar ratio of 1.82:1:1:5555 (and repeat with 0.96:1:1:5555) was stirred for 30 min at room temperature. The pH value of the mixture was set exactly at 2, 4, 6, 8 and 10 using aqueous solutions of NaOH and HCl (1 M). The mixture was transferred to a Teflon-lined stainless steel autoclave (25 mL) and the temperature was increased at the speed of 5 °C/10 min so that it became fixed at 180 °C. After 4 days, the temperature was lowered at the rate of 5 °C/10 min until it reached room temperature. At the end of the reaction, the pH of the solution did not change. The black precipitate was washed with distilled water and dried at room temperature in a desiccator. The product has a melting point of 1800 °C and is insoluble in water and other common solvents.

Results and discussions

Many factors affect the formation of nanocrystalline products. These factors generally are: the type of initial materials, molar ratio, pH values, reaction duration and temperature during the hydrothermal synthesis process. Changes of these factors have led to many reactions in many different situations. Temperature was evaluated in the range of 150–200 °C and the reaction time was evaluated in the range of 2 to 6 days and we finally concluded that suitable nanocrystals are formed at the temperature of 180 °C in 4 days. Changing the initial material from molybdenum trioxide to ammonium heptamolybdate tetrahydrate did not lead to formation of any nanocrystals.

PXRD was used for te evaluation of phase changes of the prepared nanocrystals. On the basis of X-ray diffraction pattern data, it was observed that powders synthesized by the Ni/Mo = 0.96 molar ratio of raw materials forms amorphous crystals, whereas the sample is completely crystallized using Ni/Mo = 1.82 molar ratio. This results show that synthesized nanocrystals are formed with an additional amount of $NiSO_4$.

Figure 1 shows the X-ray diffraction patterns of nanocrystals which have been synthesized with molar ratio of Ni/Mo = 1.82 at different pH values. Nanocrystals obtained at pH values less than 10 consist of two phases. The first phase is the main phase of nickel bis(*p*-phenylenediamino) [formula: $Ni(C_6H_4(NH)_2)_2$] related to JCPDS No. 00-025-1554 and the second phase is the smaller phase of $NiMoO_4$ related to JCPDS No. 00-031-0902 (the main and minor phase peaks are indicated with the * and ↑ sign, respectively, in Fig. 1). The main phase at 4, 6 and 8 pH values is monoclinic, with its first high peak at $2\theta \approx 7.010$, its second high peak at $2\theta \approx 20.498$ and its third high peak at $2\theta \approx 23.772$. At pH value of 2, the smaller phase is the dominant phase with its first high peak at $2\theta \approx 28.852$, its second high peak at $2\theta \approx 14.320$ and its third high peak at $2\theta \approx 33.762$. Small peaks which are observed to be more than 28 at 2θ are attributed to diffraction peaks of smaller phase. Existence of this phase leads to a small shift to greater angle of peaks in the main phase and, as a result, there is a little overlap in the peaks of these two phases. The intensity of the diffraction peaks increases by increasing pH values from 2 to 6 and, in contrast, the intensity of the diffraction peaks in smaller phases decreases. The intensity of peaks in the main phase is slightly reduced again at pH value of 8 and ultimately broadening of peaks at pH value of 10 indicates that the powders have become amorphous. The results suggest that neutral or low alkaline conditions of pH are more favorable

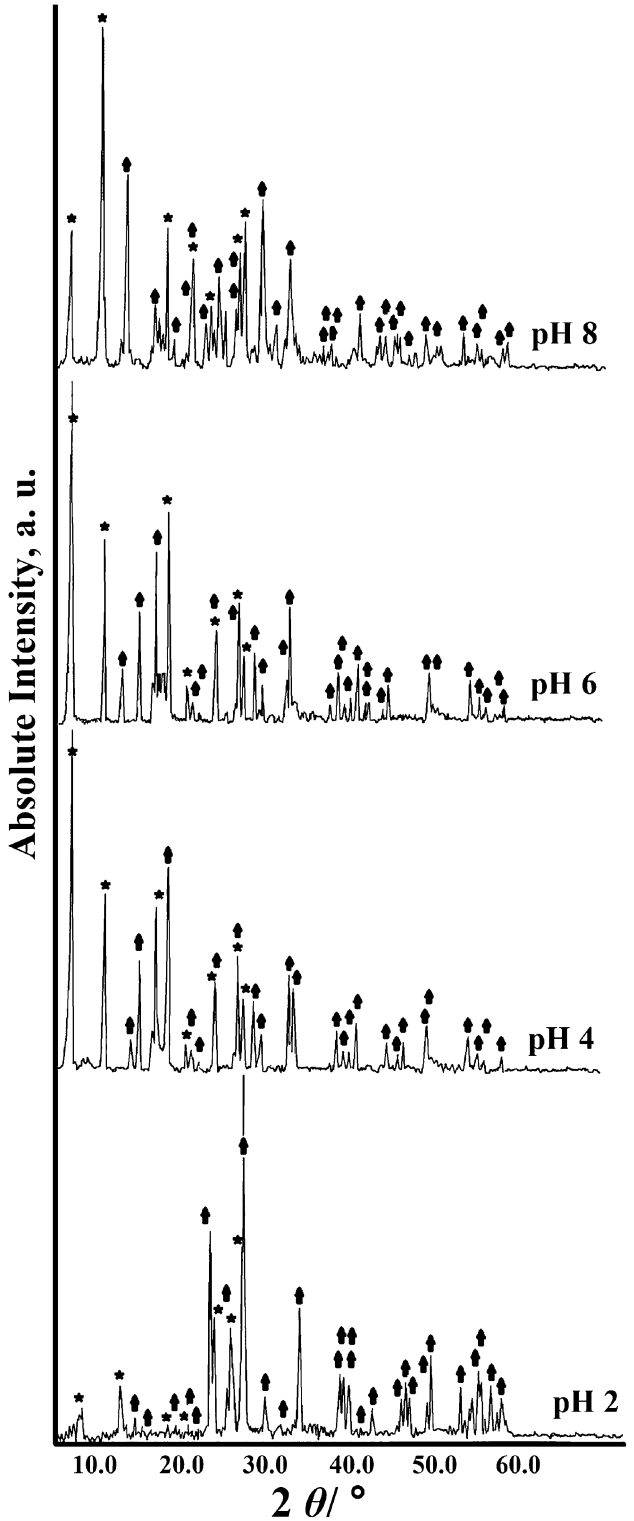

Fig. 1 XRD patterns of synthesized nanocrystals with molar ratio of Ni/Mo=1.82 at different pH values (The $Ni(C_6H_4(NH)_2)_2$ and $NiMoO_4$ phase peaks are indicated with the * and ↑ sign, respectively)

Table 1 The average crystallite sizes of the five highest diffraction peaks at different pH values

Peak no.	$D_{(pH=2)}$ (nm)	$D_{(pH=4)}$ (nm)	$D_{(pH=6)}$ (nm)	$D_{(pH=8)}$ (nm)
1	42.25	45.22	52.21	47.92
2	42.48	40.03	44.11	40.28
3	54.03	39.08	43.20	41.88
4	51.67	49.32	48.19	53.98
5	34.33	37.28	40.97	43.85

for formation of the main phase, while the smaller phase forms in acidic conditions.

The average size of crystals has been estimated using Scherrer equation:

$$D = 0.9\lambda/\beta \operatorname{Cos} \theta,$$

where D is the average diameter of the particle, λ is the CuKα radiation ($\lambda = 1.54060$ Å), β is the FWHM and θ is the Bragg's diffraction angle. The results of the highest five diffraction peaks at different pH values have been calculated using Scherrer equation and have been listed in Table 1. According to this equation, the average size of nanocrystals at different pH values was obtained in the range of 34–54 nm. The XRD results indicate that the size of crystals is increased with the increment in pH value and the pH of the initial solution affects the size of the prepared nanocrystals.

Figure 2 shows the micrographs of SEM crystals prepared with molar ratio of Ni/Mo = 1.82 at different pH values. The results shows that the morphology of the crystals changes at different pH values. The morphology of the nanocrystals is spherical with the size of 28–38 nm at pH values of 2, 4 and 10 and they are wired with the size of 35 nm at the pH value of 6. Thus, the smallest size of the crystals can be observed at pH 10 (28 nm). The SEM results suggest that the morphology of the nanostructures is changed with the increment in the pH value.

The EDX elemental analysis of products at the pH values 2–10 has been shown in Fig. 3, in which both the major and minor phases confirm the presence of Ni, Mo and PPDA. It can be concluded that the structure of the prepared compound includes PPDA spacer groups, MoO_4 units act as bridges among PPDA spacer groups and, as a result, a 3D network is formed.

The percentages and weight ratios derived from EDX elemental analysis have been listed in Table 2. The results indicate that the ratio of Ni/Mo weight percentages is increased by raising the pH value. The ratio of Ni to Mo at pH 4 and 6 are approximately 1–4.

The IR spectra obtained from pH values 2–10 (Table 3) show bands related to NH and water stretching vibration in the range of 3322–3731 cm^{-1}, C–N in the range

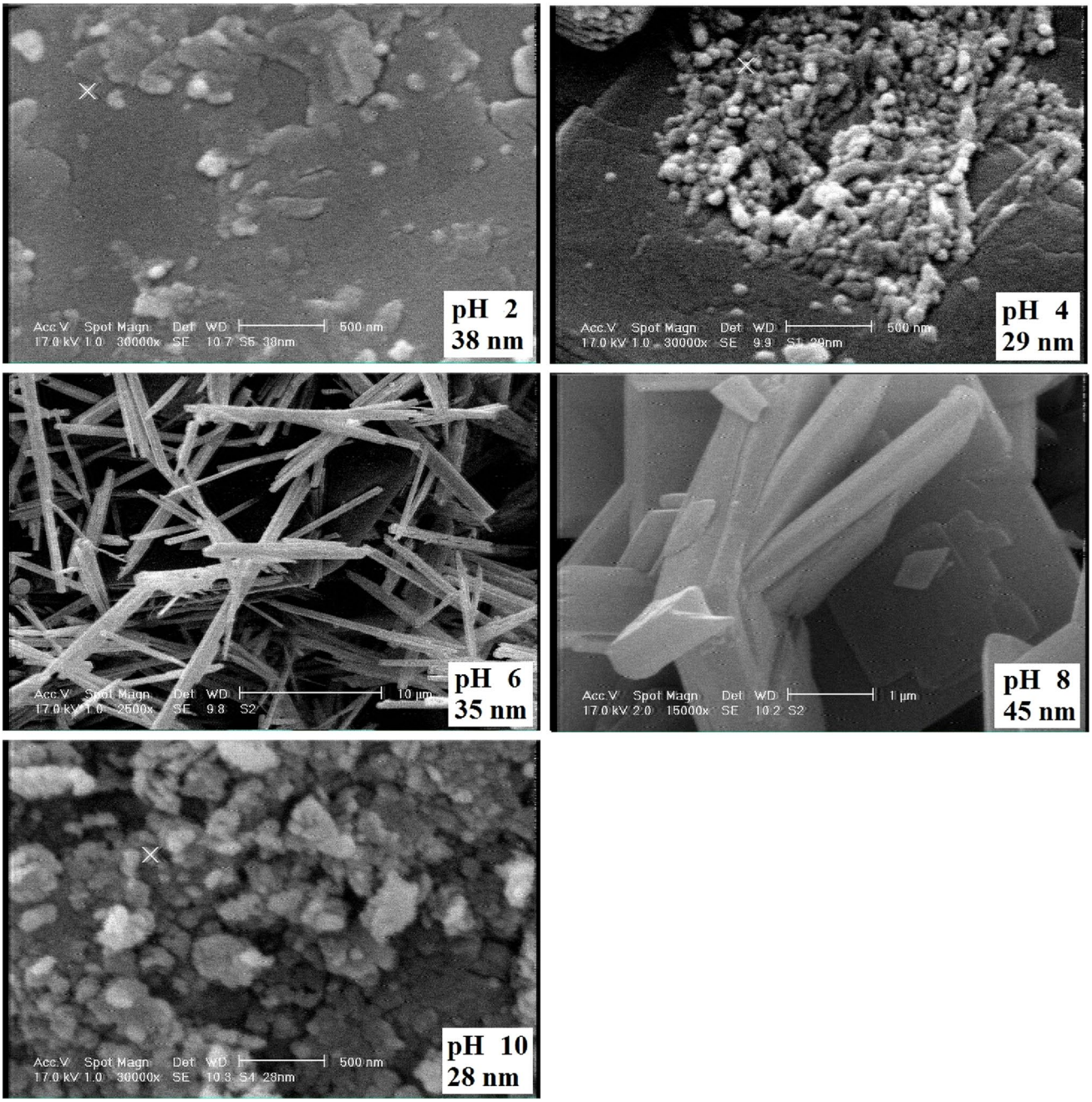

Fig. 2 SEM images of nanocrystals prepared with molar ratio of Ni/Mo = 1.82 at different pH values

of 1238–1288 cm^{-1} and C=C of PPDA ring in the range of 1509–1518 cm^{-1}. Stretching vibration bands of Ni–N and Ni–O can be observed in the ranges of 518–590 and 429–498 cm^{-1}. Symmetric and asymmetric stretching vibrations of MoO_2 groups were identified in the ranges of 819–880 and 922–969 cm^{-1}. It shows that the crystallization of nanocrystals at neutral pH environment is optimized.

Based on the obtained results, the structure of synthesized nanocrystals is shown in Fig. 4, which indicates a three-dimensional structure. In this structure, MoO_4 acts as building blocks, linked not only through direct coordination into oxo-bridged arrays but also through secondary metal sites acting as bridge in coordination complex subunits. The structure-directing role of the metal–ligand subunit shows the coordination priority of the metal and the geometric constraints ligand.

Figure 5 shows the TGA and DTA of the prepared nanocrystals at pH 6. TGA and DTA diagrams of the product are obtained at a heating rate 5 °C/min in the atmosphere and contain a two-step weight loss. The first

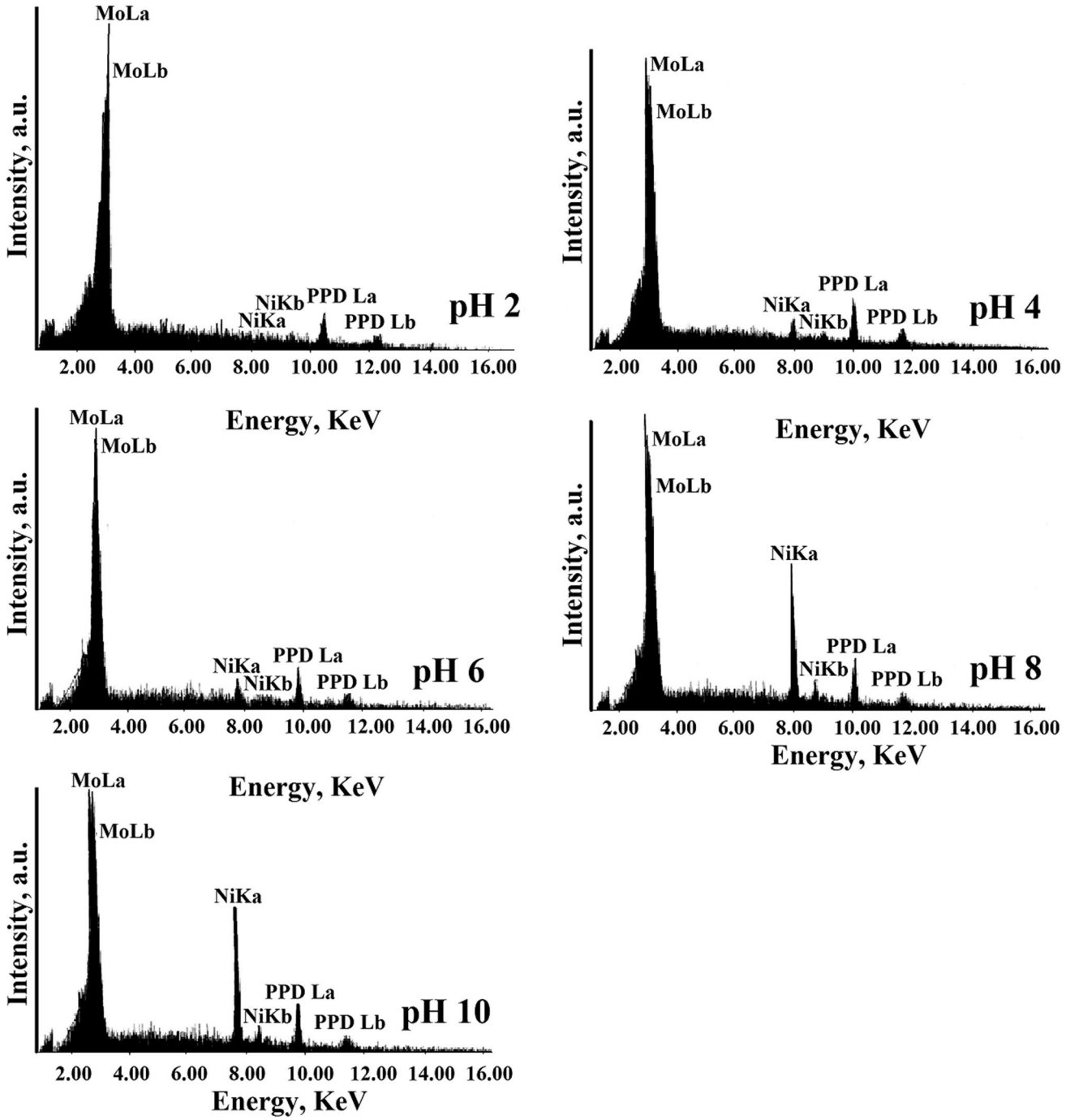

Fig. 3 EDX elemental analysis of prepared nanocrystals at the pH values 2–10

weight loss equals to 5.42% at the temperature range of 259–330 °C related to the fracture of coordinated water molecules which match the endothermic peak of 325.01 °C DTA. The second weight loss equals to 8.00% at the temperature range of 337–448 °C along with decomposition of the PPDA ligand and complex structure, which is confirmed by the exothermic peak of 420.90 °C DTA. The total weight loss of 13.42% is in agreement with the calculated data and so it has thermal resistance.

The absorbance and emission spectra of nanocrystals optimized at pH 6 in solid state at room temperature have been shown in Fig. 6. The obtained nanocrystals show an intense PL by emission peak at the wavelength of 461 nm based on excitation at the wavelength of 300 nm. Dispersing

Table 2 The percentages and weight ratios obtained from EDX elemental analysis of products at pH 2–10

pH	2	4	6	8	10
Mo (Wt%)	27.12	17.65	18.04	14.99	5.99
Ni (Wt%)	1.38	3.98	5.01	18.04	45.23
PPDA (Wt%)	71.36	83.72	76.99	66.98	46.59
Ni/Mo	0.05	0.22	0.28	1.20	7.55
Ni/PPDA	0.02	0.05	0.06	0.27	0.97

the PL light to form the spectrum indicates the structural purity of the prepared nanocrystals as well as confirms its optical properties which depend on the energy difference between the valence and conduction bands. Placement of PPDA groups between inorganic materials increases the hardness of the structure and leads to observation of PL emission as a result. In general, PL is a characteristic of the sample and is sensitive to size; therefore, the intensity of PL peak decreases by increasing particle sizes related to nanoparticles [35].

Conclusion

A new inorganic–organic hybrid compound was synthesized via the hydrothermal method using $NiSO_4$, MoO_3 and PPDA (*p*-phenylenediamine). The results indicate that MoO_4 inorganic group can be covalently connected to complexes of transition metals such as Ni-PPDA to obtain multi-dimensional structures. It was observed that the molar ratios of Ni/Mo, pH values, temperature and reaction duration effectively influence the morphology and nanostructure of final crystals. The crystal sizes increase when the pH value is increased, and particles with sizes smaller than 38 nm are formed while other parameters are fixed. On the basis of the obtained results, the crystallization of nanocrystals is controlled by a random nucleation process and is optimized at the pH value of 6. The results indicate that the ratio of Ni/Mo weight percentages is increased by raising the pH value.

Using PL spectroscopy, the optical properties of the synthesized samples, originating from the energy

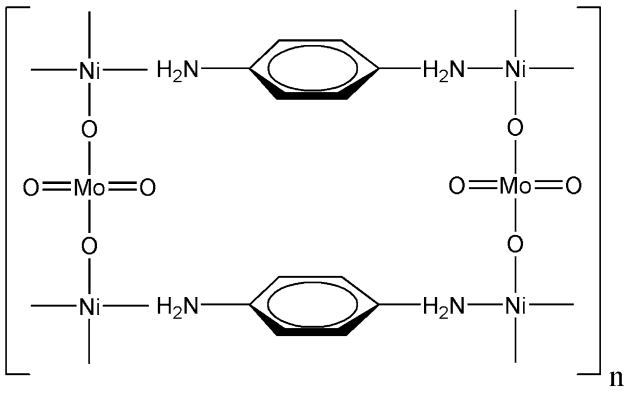

Fig. 4 The proposed structure of prepared nanocrystals at pH 6

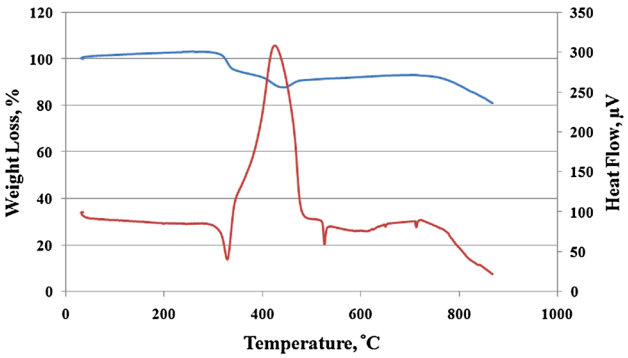

Fig. 5 The TGA-DTA thermal analysis of prepared nanocrystal at pH 6

difference between conduction and valence bands, are confirmed. Room temperature PL, which was excited at the wavelength of 300 nm, indicates a photoluminescence emission peak at the wavelength of 461 nm. The fabricated structure displays an increase in hardness as well as a photoluminescence emission due to the fact that PPDA groups locate between inorganic species. This novel inorganic–organic hybrid compound can find applications as excellent thermal stability and in nanoscience as fluorescent nanofillers with controlled functionality, shape and size.

Table 3 IR characteristic band frequencies (cm^{-1}) of the obtained compounds at different pH values

Characteristic bands	pH = 2	pH = 4	pH = 6	pH = 8	pH = 10
$\nu_{(C=C)}$	1510.23	1511.07	1510.01	1518.91	1509.25
$\nu_{(C-N)}$	1292.88	1259.99	1290.33	1240.01	1270.18
$\nu_{(NH)}$	3434.02	3376.08	3368.54	3322.93	3435.04
$\nu_{(OH)}$	3731.44	3429.75	3429.03	3397.07	3639.09
$\nu_{(MoO2)}$	819.22, 965.53	862.65, 928.98	869.17, 922.13	880.03, 969.02	869.82, 935.62
$\nu_{(Ni-N)}$	590.35	560.16	563.81	588.07	518.87
$\nu_{(Ni-O)}$	498.12	494.04	494.52	490.98	429.99

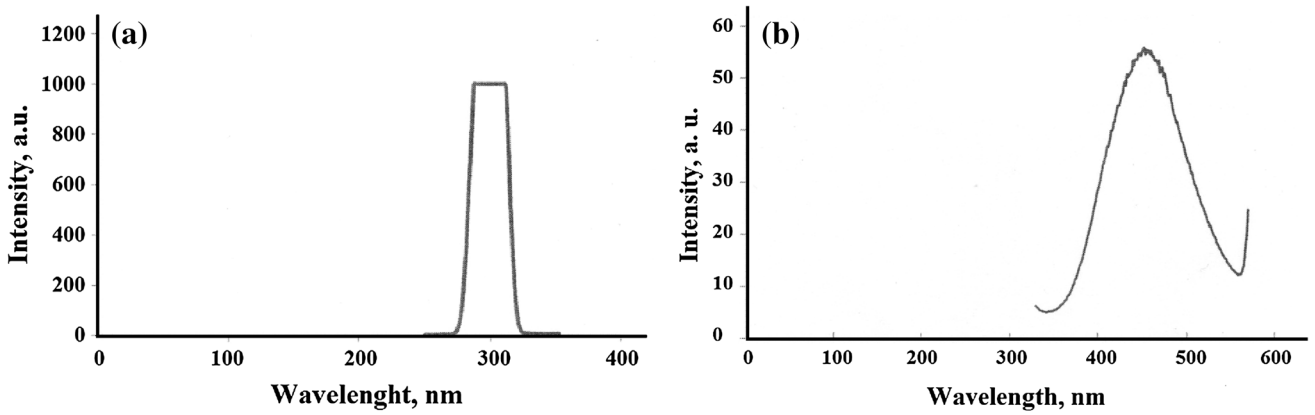

Fig. 6 The **a** absorbance and **b** emission spectra of prepared nanocrystals at pH 6 in solid state at room temperature

Open Access This article is distributed under the terms of the Creative Commons Attribution 4.0 International License (http://creativecommons.org/licenses/by/4.0/), which permits unrestricted use, distribution, and reproduction in any medium, provided you give appropriate credit to the original author(s) and the source, provide a link to the Creative Commons license, and indicate if changes were made.

References

1. Samiey, B., Cheng, C.H., Wu, J.: Organic-inorganic hybrid polymers as adsorbents for removal of heavy metal ions from solutions: a review. Materials (Basel) **7**(2), 673–726 (2014)
2. Zhang, W., Ji, X., Sun, C., Lu, X.: Fabrication and characterization of macroporous epichlorohydrin cross-linked alginate beads as protein adsorbent. Prep. Biochem. Biotechnol. **43**(5), 431–444 (2013)
3. Sanchez, C., Julian, B., Belleville, P., Popall, M.: Applications of hybrid organic–inorganic nanocomposites. J. Mater. Chem. **15**(35–36), 3559–3592 (2005)
4. Hatton, B., Landskron, K., Whitnall, W., Perovic, D., Ozin, G.A.: Past, present, and future of periodic mesoporous organosilicas the PMOs. Acc. Chem. Res. **38**(4), 305–312 (2005)
5. Michinobu, T., Kato, F., Inui, J., Nishide, H.: Two-dimensionally extended aromatic polyamines for optimization of charge-transporting properties by partial oxidation. J. Polym. Sci. Pol. Chem. **47**(18), 4577–4586 (2009)
6. Xiang, Z., Cao, D.: Synthesis of Luminescent covalent-organic polymers for detecting nitroaromatic explosives and small organic molecules. Macromol. Rapid Commun. **33**(14), 1184–1190 (2012)
7. Chang, J.-S., Hwang, J.-S., Jhung, S.H., Park, S.-E., Ferey, G., Cheetham, A.K.: Nanoporous metal-containing nickel phosphates: a class of shape-selective catalyst. Angew. Chem. Int. Ed. **43**(21), 2819–2822 (2004)
8. Perles, J., Iglesias, M., Martin-Luengo, M.A., Monge, M.A., Ruiz-Valero, C., Snejko, N.: Metal – organic scandium framework: useful material for hydrogen storage and catalysis. Chem. Mater. **17**(23), 5837–5842 (2005)
9. Sun, L.B., Kang, Y.H., Shi, Y.Q., Liu, Y., Jiang, X.Q.: Highly selective capture of the greenhouse gas CO_2 in polymers. ACS Sustainable Chem. Eng. **3**(12), 3077–3085 (2015)
10. Chang, Z., Zhang, D.-S., Chen, Q., Bu, X.-H.: Microporous organic polymers for gas storage and separation applications. Phys. Chem. Chem. Phys. **15**(15), 5430–5442 (2013)
11. Coronado, E., Galán-Mascarós, J.R., Giménez-Saiz, C., Gómez-García, C.J., Martínez-Ferrero, E., Almeida, M., Lopes, E.B., Capelli, S.C., Llusar, R.M.: New conducting radical salts based upon Keggin-type polyoxometalates and perylene. J. Mater. Chem. **14**(12), 1867–1872 (2004)
12. Coronado, E., Giménez-Saiz, C., Gómez-García, C.J., Capelli, S.C.: Metallic conductivity down to 2 K in a polyoxometalate-containing radical salt of BEDO-TTF. Angew. Chem. Int. Ed. **43**(23), 3022–3025 (2004)
13. Shi, Z., Peng, J., Gomez-Garcia, C.J., Benmansour, S., Gu, X.: Influence of metal ions on the structures of Keggin polyoxometalate-based solids: hydrothermal syntheses, crystal structures and magnetic properties. J. Solid State Chem. **179**(1), 253–265 (2006)
14. Reglero Ruiz, J.A., Trigo-López, M., García, F.C., García, J.M.: Functional aromatic polyamides. Polymers **9**(9), 414 (2017)
15. Lu, C.-Z., Wu, C.-D., Zhuang, H.-H., Huang, J.-S.: Three polymeric frameworks constructed from discrete molybdenum oxide anions and 4,4′-bpy-bridged linear polymeric copper cations. Chem. Mater. **14**(6), 2649–2655 (2002)
16. Shi, Z., Feng, S., Gao, S., Zhang, L., Yang, G., Hua, J.: Inorganic–organic hybrid materials constructed from $[(VO_2)(HPO_4)]_\infty$ helical chains and $[M(4,4'\text{-bpy})_2]^{2+}$ (M=Co, Ni) fragments. Angew. Chem. Int. Ed. **39**(13), 2325–2327 (2000)
17. Han, G.H., Lin, B.Z., Li, Z., Sun, D.Y., Liu, P.D.: Hydrothermal synthesis and characterization of a new hybrid organic–inorganic compound $[Cd(en)_3]MoO_4$. J. Mol. Struct. **741**(1), 31–35 (2005)
18. Duan, L.-M., Xu, J.-Q., Xie, F.-T., Cui, X.-B., Ding, H., Song, J.-F.: Synthesis and characterization of a new compound based on mixed Mo/V polyoxometalates connected and modified by $[Ni(en)_2]^{+2}$ groups. Mendeleev Commun. **15**(2), 79–80 (2005)
19. Wu, L., Ma, H., Han, Z., Li, C.: Synthesis, structure and property of a new inorganic–organic hybrid compound $[Cu(phen)_2][Cu(phen)H_2O]_2[Mo_5P_2O_{23}]\cdot 3.5H_2O$. Solid State Sci. **11**(1), 43–48 (2009)
20. Ma, H.-Y., Wu, L.-Z., Pang, H.-J., Meng, X., Peng, J.: Hydrothermal synthesis of two Anderson POM-supported transition metal organic–inorganic compounds. J. Mol. Struct. **967**(1–3), 15–19 (2010)
21. Niu, J.Y., Guo, D.J., Wang, J.P., Zhao, J.W.: 1D Polyoxometalate-based composite compounds derived from the Wells–Dawson subunit: synthesis and crystal structure of [{Ce(DMF)4(H2O)3}{Ce(DMF)4(H2O)4}(P2W18O62)]·H2O. Cryst. Growth Des. **4**(2), 241–247 (2004)

22. Yuan, J., Liu, X., Akbulut, O., Hu, J., Suib, S.L., Kong, J., Stellacci, F.: Superwetting nanowire membranes for selective absorption. Nat. Nanotechnol. **3**(6), 332–336 (2008)
23. Benedetto, F.D., Camposeo, A., Pagliara, S., Mele, E., Persano, L., Stabile, R., Cingolani, R., Pisignano, D.: Patterning of light-emitting conjugated polymer nanofibres. Nat. Nanotechnol. **3**(10), 614–619 (2008)
24. Zhao, X., Liu, J., Yang, H., Fan, L., Yang, S.: Novel polyfluorinated polyimides derived from α, α-bis(4-amino-3,5-difluorophenyl)phenylmethane and aromatic dianhydrides: synthesis and characterization. Eur. Polym. J. **44**(3), 808–820 (2008)
25. Zhu, Z., Waller, D., Gaudiana, R., Morana, M., Mühlbacher, D., Scharber, M., Brabec, C.: Panchromatic conjugated polymers containing alternating donor/acceptor units for photovoltaic applications. Macromolecules **40**(6), 1981–1986 (2007)
26. Jung, K.M., Kim, K.H., Jin, J.-I., Cho, M.J., Choi, D.H.: Deep-red light-emitting phosphorescent dendrimer encapsulated tris-[2-benzo[b]thiophen-2-yl-pyridyl] iridium (III) core for light-emitting device applications. J. Polym. Sci. Part A: Polym. Chem **46**(22), 7517–7533 (2008)
27. Nandia, M., Kumar Das, S., Giri, S., Bhaumik, A.: Fe(III)-containing mesoporous poly-(*p*-phenylenediamine): synthesis, characterization and magnetic properties. Micropor. Mesopor. Mat. **142**(2–3), 557–563 (2011)
28. Dolbecq, A., Mialane, P., Lisnard, L., Marrot, J., Secheresse, F.: Hybrid organic–inorganic 1D and 2D frameworks with ε-Keggin polyoxomolybdates as building blocks. Chem. Eur. J. **9**(12), 2914–2920 (2003)
29. Burkholder, E., Zubieta, J.: A two-dimensional bimetallic oxide constructed from ζ-octamolybdate clusters and Ag(I)-tpyprz cationic polymer components (tpyprz = tetra-2-pyridylpyrazine). Solid State Sci. **6**(12), 1421–1428 (2004)
30. Bu, W.-M., Ye, L., Yang, G.-Y., Gao, J.-S., Fan, Y.-G., Shao, M.-C., Xu, J.-Q.: One- and two-dimensional framework materials constructed from the mixed Mo/V tetra-capped Keggin structure clusters and $M(en)_2$ (M=Ni, Cu) complexes groups. Inorg. Chem. Commun. **4**(1), 1–4 (2001)
31. Hagrman, D., Hagrman, P., Zubieta, J.: Polyoxomolybdate clusters and copper–organonitrogen complexes as building blocks for the construction of composite solids. Inorg. Chim. Acta **300–302**, 212–224 (2000)
32. Nezamzadeh-Ejhieh, A., Salimi, Z.: Heterogeneous photodegradation catalysis of o-phenylenediamine using CuO/X zeolite. Appl. Catal. A-Gen. **390**(1–2), 110–118 (2010)
33. Wang, Q., Tang, H., Xie, Q., Jia, X., Zhang, Y., Tan, L., Yao, S.: The preparation and characterization of poly(o-phenylenediamine)/gold nanoparticles interface for immunoassay by surface plasmon resonance and electrochemistry. Colloid. Surface B **63**(2), 254–261 (2008)
34. Palys, B., Bokum, A., Rogalski, J.: Poly-o-phenylenediamine as redox mediator for laccase. Electrochim. Acta **52**(24), 7075–7082 (2007)
35. Liou, G.S., Hsiao, S.H., Su, T.H.: Synthesis, luminescence and electrochromism of aromatic poly(amine–amide)s with pendent triphenylamine moieties. J. Mater. Chem. **15**(18), 1812–1820 (2005)

Publisher's Note Springer Nature remains neutral with regard to jurisdictional claims in published maps and institutional affiliations.